

Imaging Molecular Outflow in Massive Star-forming Regions with HNC O Lines

JINJIN XIE ¹, JUAN LI ¹, JUNZHI WANG ², SHU LIU ³, KAI YANG ⁴, DONGHUI QUAN ⁵, SIQI ZHENG ^{1,6},
YUQIANG LI,^{1,6} JINGWEN WU,⁶ YAN DUAN ^{3,6} AND DI LI ^{3,5,7}

¹*Shanghai Astronomical Observatory, 80 Nandan Road, Shanghai 200030, China*

²*Guangxi Key Laboratory for Relativistic Astrophysics, Department of Physics, Guangxi University, Nanning 530004, PR China*

³*National Astronomical Observatories, Chinese Academy of Sciences, A20 Datun Road, Chaoyang District, Beijing 100101, China*

⁴*School of Astronomy and Space Science, Nanjing University, 163 Xianlin Avenue, Nanjing 210023, China*

⁵*Research Center for Intelligent Computing Platforms, Zhejiang Laboratory, Hangzhou 311100, China*

⁶*University of Chinese Academy of Sciences, Beijing 100049, China*

⁷*NAOC-UKZN Computational Astrophysics Centre, University of KwaZulu-Natal, Durban 4000, South Africa*

ABSTRACT

Protostellar outflows are considered a signpost of star formation. These outflows can cause shocks in the molecular gas and are typically traced by the line wings of certain molecules. HNC O (4–3) has been regarded as a shock tracer because of the high abundance in shocked regions. Here we present the first imaging results of HNC O (4–3) line wings toward nine sources in a sample of twenty three massive star-forming regions using the IRAM 30 m telescope. We adopt the velocity range of the full width of HC₃N (10–9) and H¹³CO⁺ (1–0) emissions as the central emission values, beyond which the emission from HNC O (4–3) is considered to be from line wings. The spatial distributions of the red- and/or blue-lobes of HNC O (4–3) emission nicely associate with those lobes of HCO⁺ (1–0) in most of the sources. High intensity ratios of HNC O (4–3) to HCO⁺ (1–0) are obtained in the line wings. The derived column density ratios of HNC O to HCO⁺ are consistent with those previously observed towards massive star-forming regions. These results provide direct evidence that HNC O could trace outflow in massive star-forming regions. This work also implies that the formation of some HNC O molecules is related to shock, either on the grain surface or within the shocked gas.

Keywords: ISM: clouds — ISM: molecules — radio lines: ISM — stars: formation

1. INTRODUCTION

Massive star-forming regions are considered to be exposed to shocks, which are powered by cloud collisions, infall motions, OB stellar winds, and ionization fronts (Motte et al. 2018). Shocks including outflows are supposed to be more vigorous in the later stages of massive star formation. Outflows usually manifest as broad line wings in spectra and spatially separated red- and/or blue-lobes centered on young stellar objects, and often show increased abundances in shock tracers such as SiO, SO, CH₃OH, NH₃, and Isocyanic acid (HNC O) (e.g. Bachiller et al. 1993; Chernin et al. 1994; Kalenskii et al. 2007; Rodríguez-Fernández et al. 2010; Li et al. 2019).

Among these shock tracers, HNC O is peculiar both chemically and astrophysically. Chemically, HNC O is a nearly prolate asymmetric top molecule and the simplest complex organic species containing C, H, O, and N elements (Jones et al. 1950). Resembling a peptide bond, HNC O has been considered among the precursors of prebiotic molecules (Bisschop et al. 2007; Ferus et al. 2018; Quénard et al. 2018). Since its first detection in Sagittarius B2 (Snyder & Buhl 1971), HNC O has been ubiquitously detected in various interstellar circumstances, from comets to external galaxies (e.g. Brown 1981; Nguyen-Q-Rieu et al. 1991; Lis et al. 1997; Velilla Prieto et al. 2015). Observations of HNC O towards dense hot clumps associated with protostars and HII regions (e.g. Li et al. 2013; Jackson et al. 2013) indicated that HNC O might be related with star formation. The role of tracing shocks has been suggested for HNC O

from its associations with other shock tracers, e.g., seen in the integrated intensities maps (Zinchenko et al. 2000; Rodríguez-Fernández et al. 2010; Sanhueza et al. 2012; Miettinen 2014). HNC spectra with broad line wings have been noticed towards low mass (Rodríguez-Fernández et al. 2010) and massive star-forming regions (Zinchenko et al. 2000; Li et al. 2013; Canelo et al. 2021). However, spatially resolved analyses on the line wings of HNC, which may be from outflows, are still lacking.

The high abundance of HNC in the shocked regions has been considered to support that HNC is a shock tracer. The abundances of HNC are typically within the range of 10^{-10} to 10^{-8} (e.g. Zinchenko et al. 2000; Bisschop et al. 2007; Quan et al. 2010). The highest value 1×10^{-7} of HNC abundance was detected towards the shocked region of L1157 (Rodríguez-Fernández et al. 2010), which is a well-studied low-mass star-forming region (e.g. Bachiller & Pérez Gutiérrez 1997; James et al. 2020). From the astrochemical prospects, the abundance of HNC could increase in warm dense gas (Kelly et al. 2017). Most recent chemical modelings introduced in shocks indicated that the abundance of HNC can be increased by one order of magnitude even in weakly shocked regions (Zhang et al. 2020). Thus, substantial HNC intensities should be observed towards shocked regions in massive star formation.

In this paper, we present the observational data from IRAM 30 m telescope towards a sample of 9 hot cores at the later stages of massive star formation. We provide the results of the line wings, the outflow lobes, and the high intensity ratios of HNC to HCO^+ , further supporting HNC as a shock tracer. Sect. 2 explains the observational parameters. Sect. 3 presents the mapping results of the HNC line wing and the derived intensity ratios of HNC (4–3) to HCO^+ (1–0) in the line wings. Comments on individual sources are given in Sect. 3.4. The results are discussed in Sect. 4. We summarize the results in Sect. 5.

2. OBSERVATION AND DATA REDUCTION

The sources are selected from a sample of 23 massive star-forming regions (Liu et al. in prep.), which have been measured trigonometric parallaxes with class II methanol masers or water masers (Reid et al. 2014) and show spatial distributions in H^{13}CN (3–2) (Liu et al. in prep.). The observed sources are listed in Table 1. The observations were done with the Instituto de Radioastronomía Milimétrica (IRAM) 30-m telescope at Pico Veleta, Spain in July, October, and November 2019, December 2020, and January 2021. The data were taken with the 3 mm (E0) band of the Eight Mixer Receiver (EMIR) and the Fourier Transform Spectrometers (FTS) backend to cover 8 GHz bandwidth with a 195 kHz spectral resolution for each band in dual polarization. The beam size of IRAM 30 m is $\sim 27''$ at 90 GHz. The typical system temperatures were around 150 K in the 3 mm band. Pointing was checked every 2 hours with nearby strong quasi-stellar objects. Focus was checked and corrected at the beginning of each run and during sunsets/sunrises. The antenna temperature (T_A^*) was converted to the main beam brightness temperature (T_{mb}) using $T_{\text{mb}} = T_A^* \cdot F_{\text{eff}} / B_{\text{eff}}$, where the forward efficiency F_{eff} is 0.95 and beam efficiency B_{eff} is 0.81 for 3 mm band. Mapping observations were carried out using the On-The-Fly (OTF) mode. The off-positions were $\sim 600''$ to the peak of each mapping region. Each scan consists of 2 minutes with an on-source integration of 1 minute. We used the CLASS package, which is a part of the GILDAS¹ software, to reduce the data. The spectra were smoothed to 1.33 km s^{-1} to improve the signal-to-noise ratio of the measured line emission. The pixel size was resampled to $9''$ for each source.

We observed HNC ($J_{Ka,Kb}=4_{0,4}-3_{0,3}$) transition (hereafter HNC (4–3)) at 87925.238 MHz. HCO^+ J=1–0 (hereafter HCO^+ (1–0)) at 89188.526 MHz and its optically thin isotope H^{13}CO^+ J=1–0 (hereafter H^{13}CO^+ (1–0)) at 86754.288 MHz are used to distinguish outflow. The observation also covered HC_3N J=10–9 (hereafter HC_3N (10–9)) at 90978.989 MHz for tracing dense gas. The HII region is represented with radio recombination line H42 α at 85688.39 MHz, which traces ionized gas. The physical parameters for the observed lines are listed in Table 2.

3. RESULTS

3.1. Line wings of HNC (4–3) emission

Fig. 1 and Fig. 2 show the spectra of the observed lines averaged from the HNC (4–3) contoured red- and/or blue-shifted emission areas, which are labeled in Fig. 3 and Fig. 4. The 3σ noise level is $\sim 0.2 \text{ K}$ at 1.33 km s^{-1} velocity resolution. HNC(4–3) line wings in most sources could be distinguished from Fig. 1 and Fig. 2. The velocity range of the line wing is determined from the whole emission above zero intensity excluding the line center emission, which is identified by visually inspecting the spectra of the optically thin lines H^{13}CO^+ (1–0) and HC_3N (10–9). The red and/or blue line wings are labeled with slashed windows in corresponding colors, as shown in Fig. 1. Fig. 1 also

¹ <http://www.iram.fr/IRAMFR/GILDAS>

includes the spectra of the two optically thin lines. In four sources, G015.03-00.67, G075.76+00.33, G109.87+02.11, and G111.54+00.77, only blue line wings are prominent. In the northern region of source G034.39+00.22, only red line wings are prominent. The rest of the sources show both red and blue line wings. For sources that lack either red- or blue-line wing, the velocity range of the line core is labeled with the black window.

HCO⁺ (1–0), a commonly used outflow/infall tracer, is also used to help distinguish outflows. The spectra of HCO⁺ (1–0) together with the two optically thin lines are included in Fig. 2. HCO⁺ (1–0) shows clear line wings in all sources. In the majority of the sources, the preferences for red- and/or blue-shifted line wings in HCO⁺ (1–0) are consistent with those in HNCO (4–3), except for G109.87+02.11 and G111.54+00.77. The velocity ranges of HNCO (4–3) and HCO⁺ (1–0) line wings are listed in Table 3. In most of the sources, the velocity range of the line wing of HNCO (4–3) is equivalent to or slightly less than that of HCO⁺ (1–0). Thus, the line wings of HNCO (4–3) are attributed to outflows.

3.2. Integrated intensities of HNCO line wings

The intensities of HNCO (4–3) line wings are integrated to depict the outflow lobes. The contours for the integrated intensities of the molecular lines in all sources shown in Fig. 3 and Fig. 4 are drawn from 3 σ level with the increment of 2 σ if not specified in the captions of the figures. The integrated intensities of HNCO (4–3) towards the line core and line wings, the integrated intensities of H¹³CO⁺ (1–0) towards the line core, and the integrated intensities of HCO⁺ (1–0) towards the line wings are listed in Table 3. The distributions of HNCO (4–3) red- and/or blue-lobes are similar to those of HCO⁺ (1–0) in most of the sources, except G111.54+00.77. Fig. 3 presents the three sources showing both red- and blue-shifted emissions of HNCO (4–3). Fig. 4 includes all other sources. The centers of the bipolar outflows traced by HNCO (4–3) and HCO⁺ (1–0) are not always at the dense cores traced by HC₃N (10–9). In G075.76+00.33 and G192.60-00.04, the red- or blue-shifted emissions of HNCO (4–3) integrated intensities are distributed adjacent to HII regions.

3.3. Intensity ratios and column density ratios of HNCO to HCO⁺

With the assumptions that the excitation conditions are similar in the line center and in the outflowing gas, the intensity ratios of HNCO (4–3) to HCO⁺ (1–0) ($I[\text{HNCO}]/I[\text{HCO}^+]$, $[\text{HNCO}]/[\text{HCO}^+]$ hereafter) in the line center and the outflowing gas can be compared. The velocity ranges of HNCO(4–3) and HCO⁺(1–0) line center and line wings are listed in Table 3, which also includes the corresponding integrated intensities of HNCO (4–3) and HCO⁺ (1–0). From Table 3, the intensity ratios of HNCO (4–3) to HCO⁺ (1–0) in the line center range from (0.28 \pm 0.01)% to (1.55 \pm 0.06)%, with the median of (0.53 \pm 0.05)%. The ranges of the intensity ratios of HNCO (4–3) to HCO⁺ (1–0) are from 9.37 \pm 1.95)% to (23.34 \pm 2.33)%, with the median of (11.29 \pm 1.58)% in the red lobes, and are from (2.97 \pm 0.66)% to (36.49 \pm 7.82)%, with the median of (11.07 \pm 3.17)% in the blue lobes.

The column density ratios of HNCO to HCO⁺ could be converted from the intensity ratios of HNCO (4–3) to HCO⁺ (1–0) assuming the molecular lines are optically thin. Under the optically thin and LTE assumptions, the column density is calculated from

$$N_{\text{tot}} = \frac{8\pi}{\lambda^3 A} \frac{g_l}{g_u} \frac{1}{J_\nu(T_{\text{ex}}) - J_\nu(T_{\text{bg}})} \frac{1}{1 - \exp(-h\nu/kT_{\text{ex}})} \times \frac{Q_{\text{rot}}}{g_l \exp(-E_l/kT_{\text{ex}})} \int T_{\text{mb}} dv, \quad (1)$$

(Vasyunina et al. 2011). λ is the rest wavelength of the transition, $\lambda \equiv c/\nu$. A is the Einstein spontaneous coefficient. g_u , the upper state total degeneracy, is given by the product of rotational and spin degeneracies: $g_u \equiv g_J g_K g_I$ (Mangum & Shirley 2015)². The values of g_u for HNCO and H¹³CO⁺ are 9 and 3, respectively. Those values are from The Cologne Database for Molecular Spectroscopy (CDMS) (Müller et al. 2001, 2005; Endres et al. 2016). E_l is the energy of the lower level from Splatalogue³. $J_\nu(T_{\text{ex}})$ and $J_\nu(T_{\text{bg}})$ are the equivalent Rayleigh-Jeans excitation and background temperatures.

$$J_\nu(T) \equiv \frac{\frac{h\nu}{k}}{\exp\left(\frac{h\nu}{kT}\right) - 1}. \quad (2)$$

Q_{rot} is the partition function. The values of Q_{rot} at two possible excitation temperatures 37.5 K and 150 K are listed with other parameters in Table 2. The assumed excitation temperature 37.5 K is consistent with NH₃ measurements

² JPL gives different value of the nuclear spin degeneracy g_I for HNCO, for the consistency, we use the value 1 for g_I of HNCO.

³ <https://splatalogue.online>

towards the hot cores (e.g. Kohno et al. 2022; Billington et al. 2019; Urquhart et al. 2019; Hernández-Hernández et al. 2014; Wienen et al. 2012). The higher excitation temperature 150 K is approximately the average temperature derived towards several hot cores in this observation (e.g. Hunter et al. 2008; Qiu et al. 2011; Navarete et al. 2019; Nguyen-Luong et al. 2020; Beuther et al. 2022). The column density ratios for $N[\text{HNCO}]/N[\text{HCO}^+]$ converting from $[\text{HNCO}]/[\text{HCO}^+]$ are 30.05 and 161.53 for the outflow line wings at excitation temperatures of 37.5 K and 150 K, respectively.

In the line center where HCO^+ becomes optically thick, the column density of HCO^+ is converted from that of H^{13}CO^+ by a factor of 50. This value is within the range of 30 to 70 dependent on the distance and the environment in the Galaxy (Wilson & Rood 1994) and similar to the conversion factor of 50 which has been used in previous observations in Purcell et al. (2006); Sanhueza et al. (2012); Vasyunina et al. (2011). An average of 55.6 for $^{12}\text{C}/^{13}\text{C}$ in all sources is derived using the most recent $(4.77 \pm 0.81)\text{R}_{\text{GC}} + (20.76 \pm 4.61)$ in Yan et al. (2022) with R_{GC} from Table 1. The column density ratios for $N[\text{HNCO}]/N[\text{HCO}^+]$ converting from $[\text{HNCO}]/[\text{HCO}^+]$ are thus 0.57 and 3.06 for the line central emission at excitation temperatures of 37.5 K and 150 K, respectively. The column density ratios for excitation temperature at 37.5 K range from $(7.92 \pm 0.30)\%$ to $(44.11 \pm 1.76)\%$ with the median of $(15.11 \pm 1.42)\%$. Table 4 only lists the results for 37.5 K considering the beam effects. The column density ratios of $N[\text{HNCO}]/N[\text{HCO}^+]$ at 150 K can be scaled from those at 37.5 K. The derived column density ratios are consistent with previous observations towards massive star-forming regions (Vasyunina et al. 2011; Sanhueza et al. 2012), where an average of $\sim 11\%$ were derived. Future observations of other transitions with higher resolution will help better constrain the excitation conditions which will give better view.

3.4. Comments on Individual Sources

The associations of the HNCO (4–3) and HCO^+ (1–0) red- and/or blue-lobes distributions suggest that outflows from star-forming activities driven by the protostellar objects, either newly-formed or deeply embedded in HII/UCHII regions, could be the plausible explanation. The possible impacts from HII regions on the photodestruction of HNCO need further investigations. In this study, the spatial distributions of red- and/or blue-lobes of HNCO (4–3) are discussed with those of the high velocity tracer HCO^+ (1–0) and previous studies to determine the possible origins of the red and/or blue line wings. A common feature for all sources is the association in the spatial distribution of the red- and/or blue-lobes of HNCO (4–3) and HCO^+ (1–0), which might indicate the same origin of line wing broadening.

G005.88-00.39 drives one of the most luminous bipolar outflows known in the Galaxy, which have been identified previously in tracers such as ^{13}CO (2–1), SiO (5–4), HCO^+ (1–0), CO (2–1), and CO (3–2) (e.g. Sollins et al. 2004; Watson et al. 2007; Hunter et al. 2008; Su et al. 2012). In this IRAM 30 m observation, HNCO (4–3) shows collimated outflows with the same direction as in HCO^+ (1–0).

G011.91-00.61 is located in an Infrared Dark Clouds (IRDCs), which have been considered to be representative of the earliest stages of massive star formation (e.g. Simon et al. 2006; Peretto & Fuller 2009; Xie et al. 2021). The central core of G011.91-00.61 is the brightest millimeter core in this IRDC (Cyganowski et al. 2011). Bipolar outflows in ^{12}CO (2–1), HCO^+ (1–0), and SiO (2–1) have been observed towards the central core (Cyganowski et al. 2011), which are consistent with the well-collimated outflows traced by HNCO (4–3) and HCO^+ (1–0) in this observation.

G012.80-00.20 resides within the W33 complex, first detected as a thermal radio source in the 1.4 GHz (Westerhout 1958). The molecular gas in the expanding shell around HII region has been suggested to be compressed, heated, and driven by the expansion of the HII region (e.g. Keto & Ho 1989; Khan et al. 2022). Several sources were identified with high angular resolution continuum mappings with SMA (Immer et al. 2014). Among those sources, the northern fainter one AGAL012.804-00.199, was suggested to drive an outflow from CO observations (Navarete et al. 2019). With the same central velocity of CO, the outflows seen in HNCO (4–3) and HCO^+ (1–0) in this observation could also be originated from AGAL012.804-00.199.

G015.03-00.67 is located at the edge of the ionization front of M17 (Chini et al. 1980). Blueshifted emissions of HNCO (4–3) and HCO^+ (1–0) are dominant in the region, which could be influenced by the Young Stellar Objects (YSOs) identified from *Spitzer* (Povich et al. 2009) and *Chandra* (Broos et al. 2007) and/or the OB stars in the open cluster NGC 6618 towards the HII regions (Bordier et al. 2022; Hoffmeister et al. 2008; Hanson et al. 1997; Chini et al. 1980). A likely driving source is AGAL015.029-00.669, which is associated with water and ClassI methanol masers and revealed to show outflow in CO (Navarete et al. 2019).

G034.49+00.22 is another source located in an IRDC, in addition to G011.91-00.61. Hot cores/UCHII regions and a B0.5 protostar have been identified towards this region (Rathborne et al. 2005; Panagia 1973). Both HNCO (4–3) and

HCO^+ (1–0) display bipolar outflow features towards the southern core. The excess $4.5\ \mu\text{m}$ emission towards the MM4 core reported by Rathborne et al. (2005) was considered to be produced by ionized gas and/or shocked gas (Chambers et al. 2009). The two dense regions depicted in HC_3N (10–9) emissions correspond to MM2 and MM4 in Rathborne et al. (2005, 2006), respectively. MM2 is associated with IRAS 18507+0121 (Shepherd et al. 2004), together with water and methanol masers (Miralles et al. 1994). Spatially overlapping blueshifted and redshifted emissions were observed towards MM2 and MM4 (Shepherd et al. 2007; Sanhueza et al. 2010). Self-absorption emissions can be seen on HCO^+ in Figure 2, which is consistent with CO (3–2) and HCO^+ spectra in Sanhueza et al. (2010). Shocks in MM2 and MM4 can also be supported by the SiO detections shown in Figure 3.

G075.76+00.33 is located at the southern rim of the HII region G075.78+0.34 coinciding with a compact core seen in HCN (Riffel & Lüdke 2010), which could be associated with a YSO seen by Cooper et al. (2013). The directions of the blue-shifted emissions of HNCO and HCO^+ are towards the southwest densest region.

G109.87+02.11 is an active massive star-forming region detected with several YSOs (Hughes & Wouterloot 1984; Rodriguez et al. 1994). The bright radio source HW2, is associated with an early-B type star (Hughes & Wouterloot 1984). Intense magnetic fields and very bright masers were inferred to be associated with HW2 (e.g. Bartkiewicz et al. 2005; Vlemmings et al. 2006, 2010). This source is the second detected RRL maser to date (Jiménez-Serra et al. 2011). A collimated, high-velocity ionized jet and pulsating outflows have been detected in $^{12}\text{CO}(2-1)$, $^{12}\text{CO}(1-0)$, and SiO(2–1) (Comito et al. 2007; Cunningham et al. 2009; Zapata et al. 2013). Though HCO^+ spectrum shows both blue- and red-shifted emission and a collimated bipolar outflow, HNCO only shows blueshifted emission.

G111.54+00.77 is related with one of the radio continuum source IRS 1 located in an optically visible HII region NGC7538 (Wynn-Williams et al. 1974; Campbell 1984; Moscadelli et al. 2009). The central star of IRS 1 was suggested to be an O7 or earlier (Campbell 1984; Puga et al. 2010; Sandell et al. 2020). An inverse P-Cygni profile indicative of infall was seen in HNCO ($10_{0,10}-9_{0,9}$) (Qiu et al. 2011). While still accreting mass, this very young star is considered to be the driving source of an ionized jet and the hypercompact HII region (Sandell et al. 2020). The distribution of HNCO (4–3) shows a similar shape to the previously identified bubble-shape in C^{17}O (3–2), H^{13}CO^+ (4–3), continuum ($\sim 340\ \text{GHz}$), and CII emission (Qiu et al. 2011; Frau et al. 2014; Beuther et al. 2022). These morphology features could be resulted from protostellar feedback (Frau et al. 2014) and/or the strong FUV radiation (Sandell et al. 2020). The FUV radiation indicated by CII emission from PDR could destroy HNCO that shapes HNCO emission into a bubble. The spatial distributions of HNCO blue lobes show different morphologies from those of HCO^+ blue lobes, which could be most likely due to the low signal to noise ratio. The intrinsic differences in astrochemical properties could also contribute to the morphological differences between the HNCO and HCO^+ blue lobes.

G192.60-00.04 is within Sh 2-255, the optically bright HII region first cataloged by Sharpless (1959). The northern region of the mapping in this observation is adjacent to S255 N, which hosts a UCHII region and is associated with methanol and water masers (Zinchenko et al. 2012; Kurtz et al. 2004; Cyganowski et al. 2007; Zemlyanukha et al. 2018). S255 N was considered to drive a collimated outflow (Miralles et al. 1997; Cyganowski et al. 2007), while global collapse was observed in HCO^+ (3–2) (Minier et al. 2007). The center of the northern region corresponds to S255N-SMA6 in Zinchenko et al. (2012), where broad SiO emission feature and CO outflow were detected (Zinchenko et al. 2012). The southern region is related to S255 IR, a hot core associated with methanol and water masers (Goddi et al. 2007; Rygl et al. 2010), as well as several compact HII regions (Snell & Bally 1986). Disc-mediated accretion has been proposed to explain the multiple burst events observed in radio to optical bands towards YSO in this region (e.g. Fujisawa et al. 2015; Caratti o Garatti et al. 2017; Liu et al. 2018). Higher transitions of HNCO (10–9) were detected towards S255 IR (Wang et al. 2011; Zinchenko et al. 2015), where an abundance of $\sim 10^{-8}$ was derived for HNCO (Zinchenko et al. 2015). The northeast to southwest collimated bipolar outflows seen in CO and H_2 (Wang et al. 2011) are consistent with the HCO^+ outflow direction in this observation.

4. DISCUSSION

4.1. Velocity ranges of the line wings

The velocity ranges of HNCO (4–3) line wings appear smaller than that of other shock tracers (e.g. Zinchenko et al. 2000; Rodríguez-Fernández et al. 2010; Sánchez-Monge et al. 2013). The line wings of HCO^+ (1–0) listed in Table 3 are larger than those of HNCO (4–3) by $7\ \text{km s}^{-1}$ on average. In three sources, red- or blue-shifted emissions are seen in HCO^+ (1–0), but not in HNCO (4–3). The critical density of HCO^+ ($10^4-10^5\ \text{cm}^{-3}$) (Shirley 2015) is about one order of magnitude lower than that of HNCO ($10^5-10^6\ \text{cm}^{-3}$) (Nguyen-Q-Rieu et al. 1991), which could explain the excess of red and/or blue line wing in HCO^+ (1–0).

The line wings of HNC(4–3), as well as HCO^+ (1–0), are determined from comparisons on the intensities with optically thin tracers HC_3N (10–9) and H^{13}CO^+ (1–0). However, HC_3N (10–9) or H^{13}CO^+ (1–0) might not always be optically thin and unaffected by outflows. Red- and blue-line wings can be distinguished on HC_3N (10–9) profiles towards G011.91-00.61. A similar feature has been observed towards low-mass star-forming region L1157 (Beltrán et al. 2004) where HC_3N abundance got enhanced by a factor of 25 and 50 (Bachiller & Pérez Gutiérrez 1997; Mendoza et al. 2018). The factor of HNC abundance enhancement towards the same source was derived to be 6–83 (Rodríguez-Fernández et al. 2010). Chemical modeling which includes shock code supported HC_3N could be produced by gas phase reactions when shock passes (Mendoza et al. 2018). For another optically thin tracer H^{13}CO^+ (1–0), the clear red-shifted line wing towards G005.89-00.39 and a blue-shifted peak with a red-shifted shoulder as described in De Vries & Myers (2005) could be identified towards G109.87+02.11. The possible line wings of HC_3N (10–9) and H^{13}CO^+ (1–0) might result in an underestimate of the line wing ranges of HNC(4–3) and HCO^+ (1–0).

4.2. Formation mechanism in shocks

The formation mechanism of HNC, a peptide link ($-\text{NH}-\text{C}(=\text{O})-$) molecular specie essential to living systems, has drawn attention to chemical modelings, including gas-phase reactions (e.g. Iglesias 1977), grain surfaces models (e.g. Quan et al. 2010), and those involving shocks (e.g. Zhang et al. 2020). The observed line wings and the substantial intensities in the line wings of HNC in these sources are most likely resulted from shocks, which play the role in both sputtering HNC from dust grains and forming HNC in the gas-phase (Rodríguez-Fernández et al. 2010; Burkhardt et al. 2016). Prior to heating or the arrival of shocks, the relatively long timescale allows a variety of chemical reactions to form HNC on grain surfaces even at low temperatures. It has been recognized that the major formation mechanism for HNC on dust grains is the isocyanate radical NCO accreted onto the grain to react with the surface hydrogen, which is relatively free compared to larger molecular species at low temperatures (Garrod et al. 2008; Quan et al. 2010). Another formation mechanism involving thermal reaction $\text{NH} + \text{CO} \rightarrow \text{HNC}$ is also plausible in hot cores (Garrod et al. 2008; Tideswell et al. 2010). Shocks, even at low velocity, can efficiently release the abundant HNC from dust grains into gas-phase (Quan et al. 2010; Zhang et al. 2020). The temperature in the shocked gas then enables the efficient hydrogenation of NCO (Zinchenko et al. 2000; Rodríguez-Fernández et al. 2010). The abundance of HNC is also considered to be related to shock age and the grain mantle composition at the time of shock arrival (Rodríguez-Fernández et al. 2010; Zhang et al. 2020). High intensity ratios of HNC to HCO^+ in the line wings could be explained from the recent shock chemical modeling results that the abundance of HNC can be increased even in weakly shocked regions (Zhang et al. 2020). Further detailed chemistry modelings are needed to fully understand HNC in the shocks in these hot cores.

5. SUMMARY

We carried out mapping observations of HNC, HCO^+ , HC_3N , and $\text{H42}\alpha$ toward nine hot cores in a sample of twenty three sources from Reid et al. (2014) with the IRAM 30 m telescope. The main results are:

1. The line wing emissions of HNC are imaged for the first time. We found that the spatial distributions of the red- and/or blue-lobes of HNC emission nicely associate with those lobes of HCO^+ emission, indicating that HNC is a good tracer of outflow.
2. High intensity ratios of HNC(4–3) to HCO^+ (1–0) are derived in the line wings, suggesting that HNC could efficiently form in the shock environment.
3. The derived column density ratios of HNC to HCO^+ in the line center, ranging from $(7.92 \pm 0.38)\%$ to $(44.11 \pm 1.76)\%$, are consistent with those previously observed towards high-mass star-forming regions.

ACKNOWLEDGMENTS

We would like to thank the anonymous referee for his/her critical comments and constructive suggestions, which has significantly improved this work. This work is supported by the national Key R&D Program of China (No. 2022YFA1603101), the National Natural Science Foundation of China (NSFC, Grant No. 11988101 and No. U1731237). This study is based on observations carried out under project number 042-19, 147-19, and 127-20 with the IRAM 30-m telescope. IRAM is supported by INSU/CNRS (France), MPG (Germany), and IGN (Spain).

Facilities: IRAM

Software: `class`([Pety 2005](#))

Table 1. Source information and observing parameters

Source	Alias	R.A.	Decl.	Region Type	D (kpc)	R_{GC} (kpc)	Mapping Size	Reference
G05.88-00.39	W28	18:00:30.31	-24:04:04.5	UCHII	3.0	5.3	80'' \times 90''	Sato et al. (2014)
G011.91-00.61	IRDC G11.92-0.61	18:13:59.72	-18:53:50.3	HMP0	3.4	5.1	90'' \times 130''	Sato et al. (2014)
G012.80-00.20	W33 Main	18:14:14.23	-17:55:40.5	UCHII	2.9	5.5	100'' \times 100''	Immer et al. (2013)
G015.03-00.67	M17	18:20:22.01	-16:12:11.3	HCHII	2.0	6.4	100'' \times 100''	Xu et al. (2011)
G034.39+00.22	IRDC G34.43+0.24 MM4	18:53:19.00	+01:24:50.8	UCHII	1.6	7.1	90'' \times 100''	Kurayama et al. (2011)
G075.76+00.33	Onsala 2	20:21:41.09	+37:25:29.3	HII	3.5	8.2	100'' \times 100''	Xu et al. (2013)
G109.87+02.11	CepA HW 2	22:56:18.10	+62:01:49.5	UCHII	0.7	8.6	100'' \times 100''	Moscadelli et al. (2009)
G111.54+00.77	NGC7538 IRS1	23:13:45.36	+61:28:10.6	UCHII	2.6	9.6	100'' \times 100''	Moscadelli et al. (2009)
G192.60-00.04	S255	06:12:54.02	+17:59:23.3	UCHII	1.6	9.9	100'' \times 100''	Rygl et al. (2010)

Table 2. Physical parameters for HNCO, HCO⁺, H¹³CO⁺, and HC₃N

Molecular Line	λ cm	A $10^{-5} s^{-1}$	B_0 MHz	E_l/k K	Q_{rot} 37.5 K	Q_{rot} 150 K
HNCO (4–3)	0.340963	0.878011	11071.7	6.32914	117.3039	2820.206
HCO ⁺ (1–0)	0.336133	4.18697	44594.4	0	17.8601	70.4887
H ¹³ CO ⁺ (1–0)	0.345565	3.85389	43377.3	0	18.3516	72.4065
HC ₃ N (10–9)	90978.989	5.8125	4549.059	19.64782	172.1063	687.5086

Table 3. Velocity ranges and integrated intensities for HNC(4-3) and $\text{HCO}^+(1-0)^a$ towards the center and lobes

Source	center				red				blue			
	HNC(4-3) km s ⁻¹	I_{HNC} K km s ⁻¹	I_{HCO^+} K km s ⁻¹	I_{HCO^+} K km s ⁻¹	HNC(4-3) km s ⁻¹	I_{HNC} K km s ⁻¹	I_{HCO^+} K km s ⁻¹	I_{HCO^+} K km s ⁻¹	HNC(4-3) km s ⁻¹	I_{HNC} K km s ⁻¹	I_{HCO^+} K km s ⁻¹	I_{HCO^+} K km s ⁻¹
G05.88-00.39	[5,15]	2.33±0.11	16.78±0.19	[15,27]	1.22±0.12	[15,40]	12.22±0.45	[-17,5]	0.72±0.16	[-20,5]	24.22±0.43	
G011.91-00.61	[30,42]	3.80±0.12	4.91±0.12	[42,55]	1.34±0.13	[42,55]	5.74±0.13	[18,30]	1.03±0.12	[18,30]	5.36±0.12	
G012.80-00.20	[32,41]	3.20±0.29	11.19±0.23	[41,45]	0.70±0.19	[41,49]	8.67±0.28	[28,32]	0.86±0.19	[28,32]	8.03±0.20	
G015.03-00.67	[16,24]	2.00±0.12	10.73±0.13	-	-	[24,30]	3.50±0.39	[0,16]	0.80±0.16	[10,16]	6.53±0.39	
G034.39+00.22 MM2	[53,63]	1.22±0.11	5.00±0.14	[63,70]	0.49±0.10	[63,80]	5.23±0.21	-	-	-	-	
G034.39+00.22 MM4	[53,64]	3.27±0.13	8.09±0.13	[64,68]	0.49±0.08	[64,75]	3.89±0.14	[51,53]	0.27±0.05	[50,53]	0.74±0.08	
G075.76+00.33	[-6,3]	0.87±0.20	4.32±0.20	-	-	-	-	[-24,-6]	0.93±0.28	[-15,-6]	7.82±0.22	
G109.87+02.11	[-15,-8]	1.10±0.15	7.85±0.17	-	-	[-8,5]	28.52±0.25	[-23,-15]	0.85±0.16	[-40,-15]	14.97±0.35	
G111.54+00.77	[-63,-53]	1.10±0.12	2.82±0.20	-	-	[-53,-47]	8.03±0.19	[-75,-63]	0.67±0.19	[-73,-62]	6.05±0.23	
G192.60-00.04	[5,10]	0.59±0.09	1.28±0.10	[10,16]	0.39±0.12	[10,13]	2.81±0.09	[1,5]	0.08±0.08	[1,5]	2.55±0.10	

Notes: ^a The integrated intensities of $\text{HCO}^+(1-0)$ towards the center are derived from $I_{\text{H}^{13}\text{CO}^+}$ by multiplying a conversion factor of 50.

Table 4. Column Density Ratios $N[HNC0]/N[HCO^+]$ towards the line center at 37.5 K

Source	center
G05.88-00.39	(7.92±0.38)%
G011.91-00.61	(44.11±1.76)%
G012.80-00.20	(16.30±1.52)%
G015.03-00.67	(10.62±0.65)%
G034.39+00.22 MM2	(13.91±1.31)%
G034.39+00.22 MM4	(23.04±0.99)%
G075.76+00.33	(11.47±2.69)%
G109.87+02.11	(7.99±1.10)%
G111.54+00.77	(22.23±2.90)%
G192.60-00.04	(26.27±4.50)%

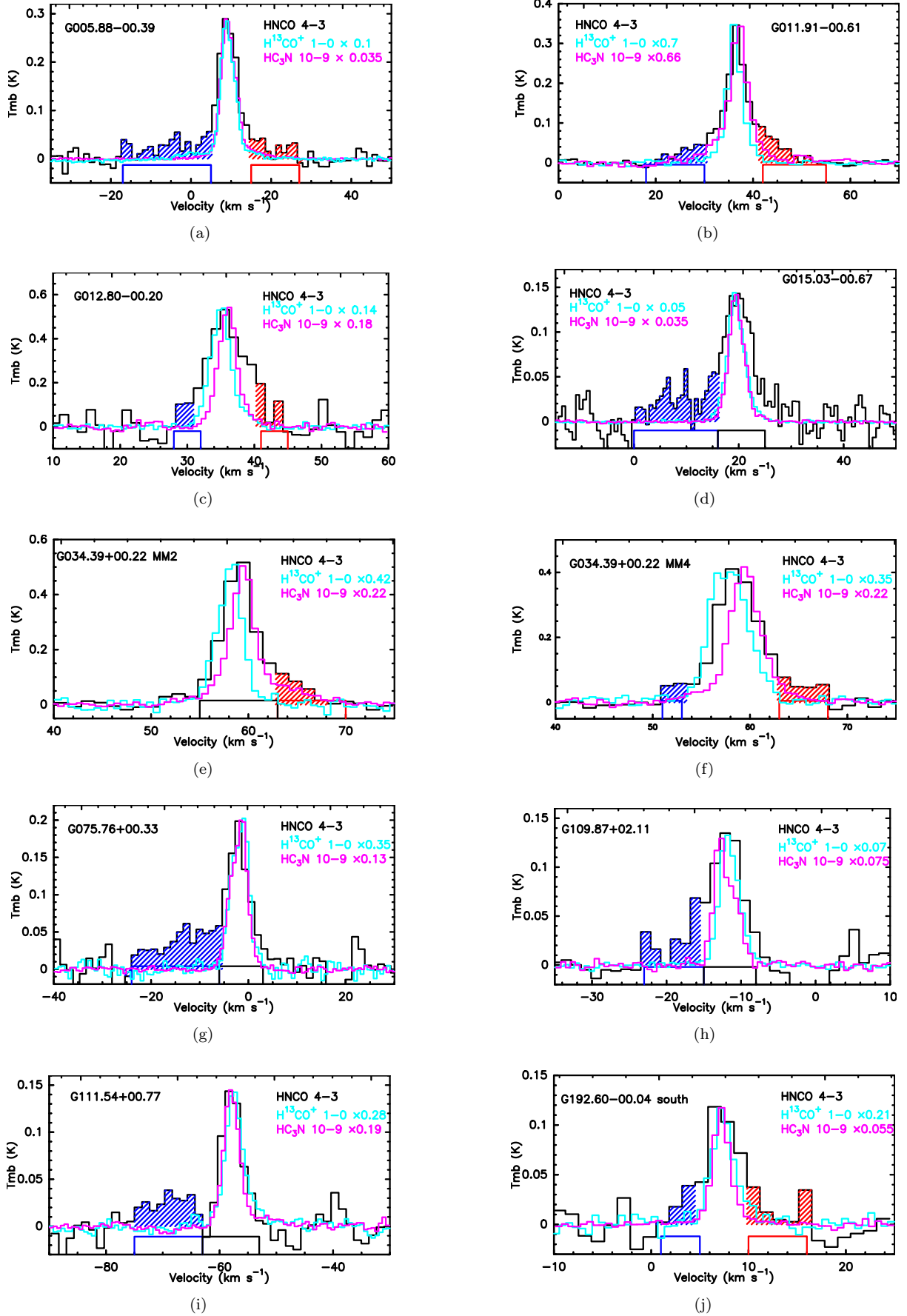


Figure 1. The spectra of HC_3N (10-9) and H^{13}CO^+ (1-0) normalized to the peak intensity of HNC (4-3) towards each source. The blue and red line wing emissions are labelled with blue and red windows. The black windows refer to the line core emission ranges. MM2 and MM4 in (e) and (f) refer to the two dust cores identified in Rathborne et al. (2005).

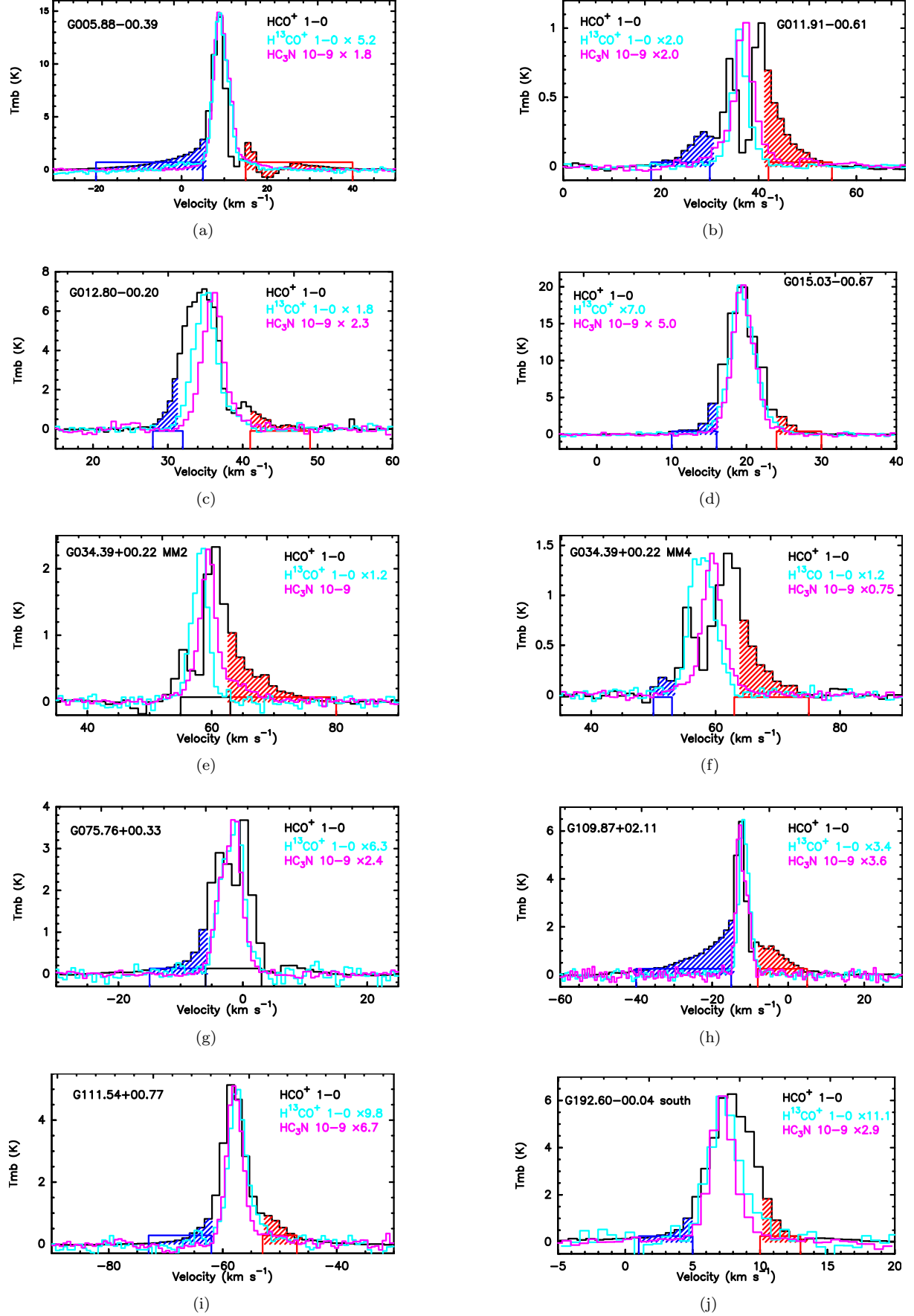


Figure 2. The spectra of HC_3N (10-9) and H^{13}CO^+ (1-0) normalized to the peak intensity of HCO^+ (1-0) towards each source. The blue and red line wing emissions are labelled with blue and red windows. The black windows refer to the line core emission ranges. MM2 and MM4 in (e) and (f) refer to the two dust cores identified in Rathborne et al. (2005).

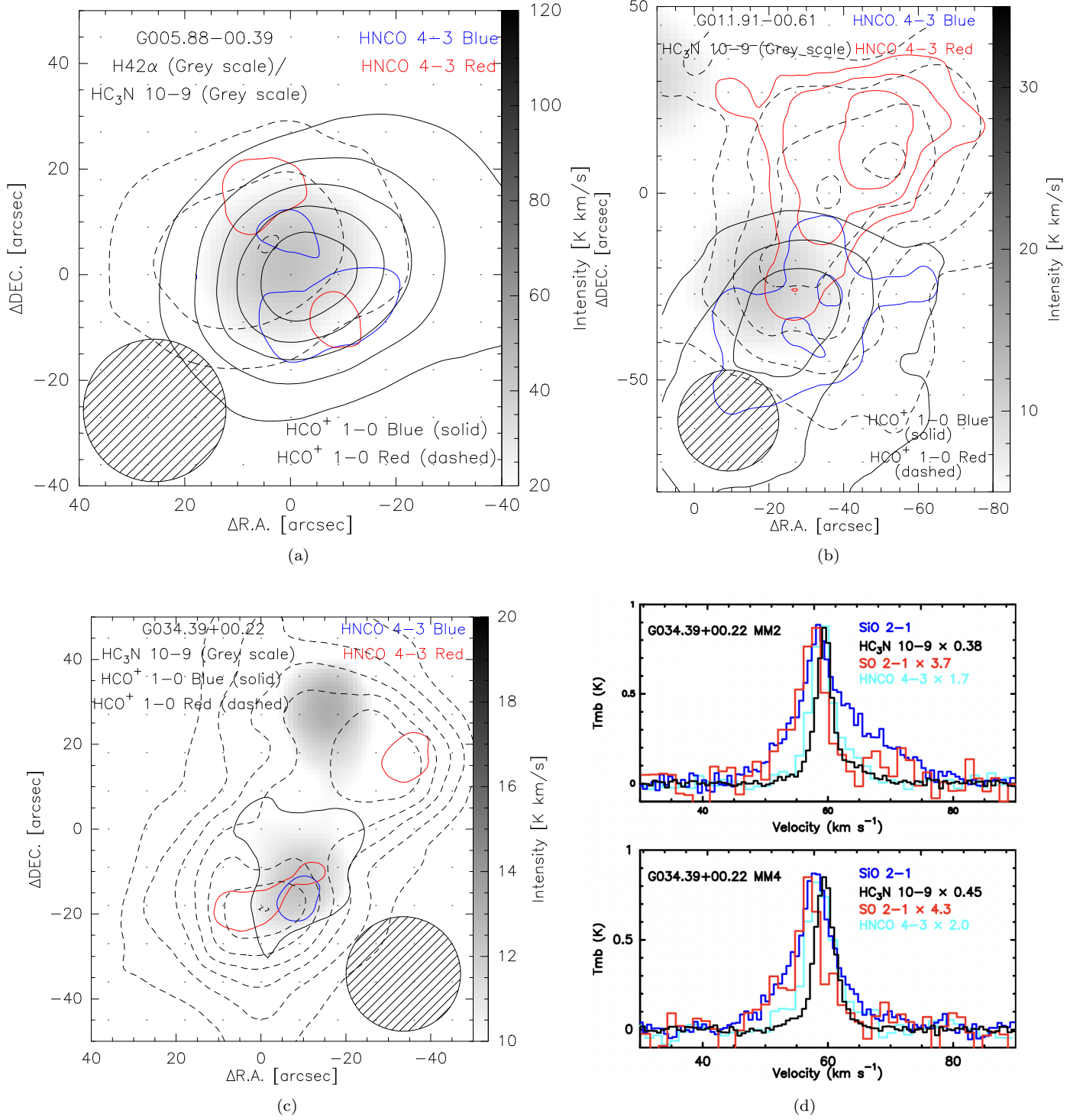


Figure 3. The blue and red line wing integrated intensities of HNC O (in blue and red, respectively) and HCO⁺ (in solid and dashed line, respectively) overlaid with H42 α and HC₃N (in grey scale) for sources labelled as outflow sources. The integrated intensities of HNC O blue and red lobes start from 3σ noise level and increase by 2σ . The integrated intensities of HCO⁺ blue and red lobes start from 5σ noise level and increase by 5σ , except for G034.39+00.22 where they start from 5σ noise level and increase by 2σ . The beam size is labelled as slash filled circle at the corner of each figure. The greyscale regions represent both H42 α and HC₃N integrated intensities, which have same scale level in source G005.88-00.39 and G011.91-00.61. For G034.39+00.22, the spectra of SO, HNC O and HC₃N normalized to SiO towards MM2 and MM4 are presented in (d). MM2 and MM4 in (d) refer to the two dust cores identified in Rathborne et al. (2005).

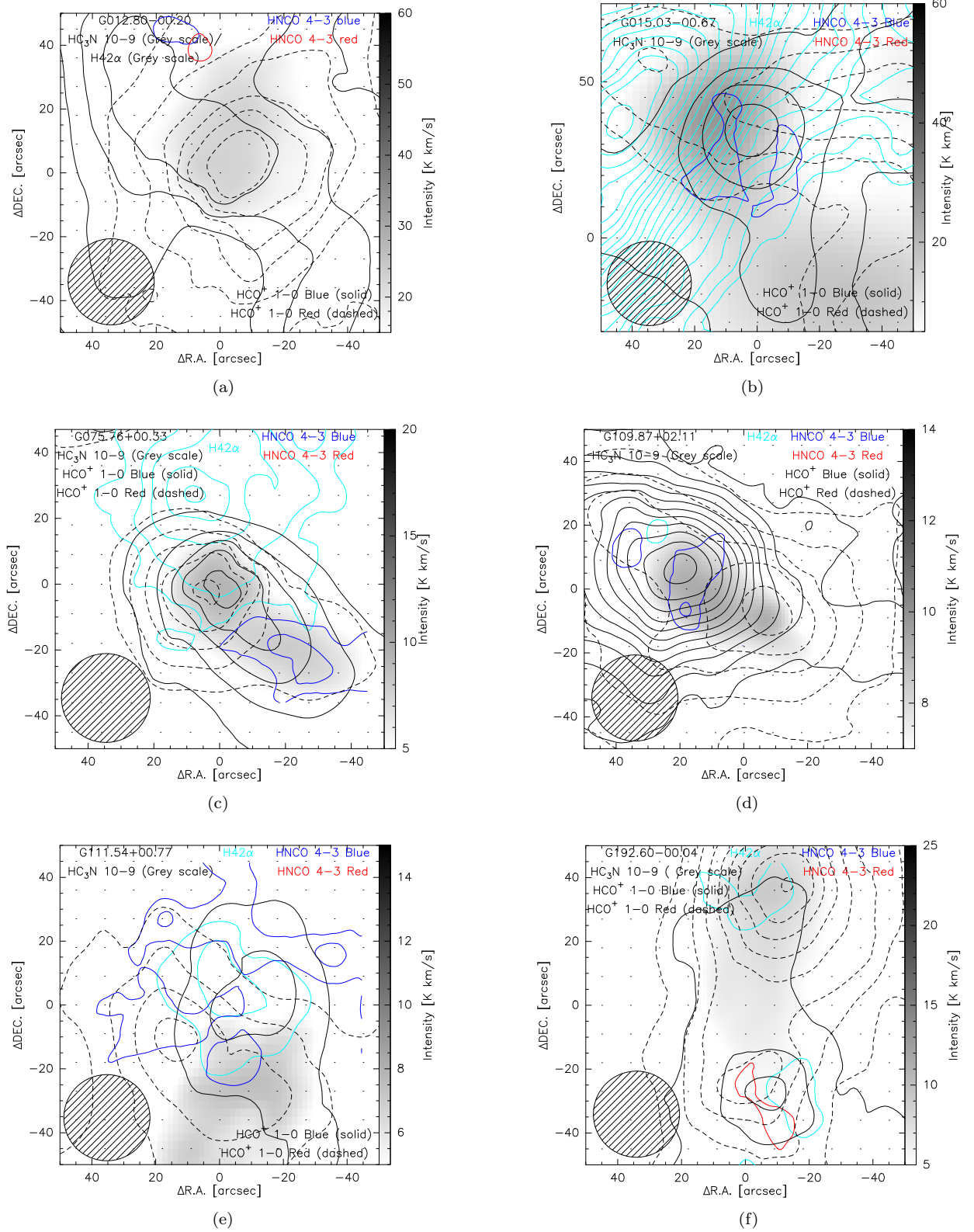


Figure 4. The blue and red line wing integrated intensities of HNCO (in blue and red, respectively) and HCO⁺ (in solid and dashed line, respectively) overlaid with H42α and HC₃N (in grey scale) for sources labelled as outflow sources. The integrated intensities of HNCO start from 3σ noise level and increase by 2σ. The integrated intensities of HCO⁺ start from 5σ noise level and increase by 5σ. The contours of H42α integrated intensity start from 5σ and increase by 5σ, except for source G012.80-00.20 where H42α is shown in grey scale as the same level as HC₃N. The beam size is labelled as slash filled circle at the corner of each figure.

REFERENCES

- Bachiller, R., Martin-Pintado, J., & Fuente, A. 1993, *ApJL*, 417, L45, doi: [10.1086/187090](https://doi.org/10.1086/187090)
- Bachiller, R., & Pérez Gutiérrez, M. 1997, *ApJL*, 487, L93, doi: [10.1086/310877](https://doi.org/10.1086/310877)
- Bartkiewicz, A., Szymczak, M., Cohen, R. J., & Richards, A. M. S. 2005, *MNRAS*, 361, 623, doi: [10.1111/j.1365-2966.2005.09203.x](https://doi.org/10.1111/j.1365-2966.2005.09203.x)
- Beltrán, M. T., Gueth, F., Guilloteau, S., & Dutrey, A. 2004, *A&A*, 416, 631, doi: [10.1051/0004-6361:20034123](https://doi.org/10.1051/0004-6361:20034123)
- Beuther, H., Schneider, N., Simon, R., et al. 2022, *A&A*, 659, A77, doi: [10.1051/0004-6361/202142689](https://doi.org/10.1051/0004-6361/202142689)
- Billington, S. J., Urquhart, J. S., Figura, C., Eden, D. J., & Moore, T. J. T. 2019, *MNRAS*, 483, 3146, doi: [10.1093/mnras/sty3053](https://doi.org/10.1093/mnras/sty3053)
- Bisschop, S. E., Jørgensen, J. K., van Dishoeck, E. F., & de Wachter, E. B. M. 2007, *A&A*, 465, 913, doi: [10.1051/0004-6361:20065963](https://doi.org/10.1051/0004-6361:20065963)
- Bordier, E., Frost, A. J., Sana, H., et al. 2022, *A&A*, 663, A26, doi: [10.1051/0004-6361/202141849](https://doi.org/10.1051/0004-6361/202141849)
- Broos, P. S., Feigelson, E. D., Townsley, L. K., et al. 2007, *ApJS*, 169, 353, doi: [10.1086/512068](https://doi.org/10.1086/512068)
- Brown, R. L. 1981, *ApJL*, 248, L119, doi: [10.1086/183638](https://doi.org/10.1086/183638)
- Burkhardt, A. M., Dollhopf, N. M., Corby, J. F., et al. 2016, *ApJ*, 827, 21, doi: [10.3847/0004-637X/827/1/21](https://doi.org/10.3847/0004-637X/827/1/21)
- Campbell, B. 1984, *ApJL*, 282, L27, doi: [10.1086/184297](https://doi.org/10.1086/184297)
- Canelo, C. M., Bronfman, L., Mendoza, E., et al. 2021, *MNRAS*, 504, 4428, doi: [10.1093/mnras/stab1163](https://doi.org/10.1093/mnras/stab1163)
- Caratti o Garatti, A., Stecklum, B., Garcia Lopez, R., et al. 2017, *Nature Physics*, 13, 276, doi: [10.1038/nphys3942](https://doi.org/10.1038/nphys3942)
- Chambers, E. T., Jackson, J. M., Rathborne, J. M., & Simon, R. 2009, *ApJS*, 181, 360, doi: [10.1088/0067-0049/181/2/360](https://doi.org/10.1088/0067-0049/181/2/360)
- Chernin, L. M., Masson, C. R., & Fuller, G. A. 1994, *ApJ*, 436, 741, doi: [10.1086/174947](https://doi.org/10.1086/174947)
- Chini, R., Elsaesser, H., & Neckel, T. 1980, *A&A*, 91, 186
- Comito, C., Schilke, P., Endesfelder, U., Jiménez-Serra, I., & Martín-Pintado, J. 2007, *A&A*, 469, 207, doi: [10.1051/0004-6361:20077408](https://doi.org/10.1051/0004-6361:20077408)
- Cooper, H. D. B., Lumsden, S. L., Oudmaijer, R. D., et al. 2013, *MNRAS*, 430, 1125, doi: [10.1093/mnras/sts681](https://doi.org/10.1093/mnras/sts681)
- Cunningham, N. J., Moeckel, N., & Bally, J. 2009, *ApJ*, 692, 943, doi: [10.1088/0004-637X/692/2/943](https://doi.org/10.1088/0004-637X/692/2/943)
- Cyganowski, C. J., Brogan, C. L., & Hunter, T. R. 2007, *AJ*, 134, 346, doi: [10.1086/518740](https://doi.org/10.1086/518740)
- Cyganowski, C. J., Brogan, C. L., Hunter, T. R., Churchwell, E., & Zhang, Q. 2011, *ApJ*, 729, 124, doi: [10.1088/0004-637X/729/2/124](https://doi.org/10.1088/0004-637X/729/2/124)
- De Vries, C. H., & Myers, P. C. 2005, *ApJ*, 620, 800, doi: [10.1086/427141](https://doi.org/10.1086/427141)
- Endres, C. P., Schlemmer, S., Schilke, P., Stutzki, J., & Müller, H. S. P. 2016, *Journal of Molecular Spectroscopy*, 327, 95, doi: [10.1016/j.jms.2016.03.005](https://doi.org/10.1016/j.jms.2016.03.005)
- Ferus, M., Laitl, V., Knizek, A., et al. 2018, *A&A*, 616, A150, doi: [10.1051/0004-6361/201833003](https://doi.org/10.1051/0004-6361/201833003)
- Frau, P., Girart, J. M., Zhang, Q., & Rao, R. 2014, *A&A*, 567, A116, doi: [10.1051/0004-6361/201423917](https://doi.org/10.1051/0004-6361/201423917)
- Fujisawa, K., Yonekura, Y., Sugiyama, K., et al. 2015, *The Astronomer's Telegram*, 8286, 1
- Garrod, R. T., Widicus Weaver, S. L., & Herbst, E. 2008, *ApJ*, 682, 283, doi: [10.1086/588035](https://doi.org/10.1086/588035)
- Goddi, C., Moscadelli, L., Sanna, A., Cesaroni, R., & Minier, V. 2007, *A&A*, 461, 1027, doi: [10.1051/0004-6361:20066136](https://doi.org/10.1051/0004-6361:20066136)
- Hanson, M. M., Howarth, I. D., & Conti, P. S. 1997, *ApJ*, 489, 698, doi: [10.1086/304808](https://doi.org/10.1086/304808)
- Hernández-Hernández, V., Zapata, L., Kurtz, S., & Garay, G. 2014, *ApJ*, 786, 38, doi: [10.1088/0004-637X/786/1/38](https://doi.org/10.1088/0004-637X/786/1/38)
- Hoffmeister, V. H., Chini, R., Scheyda, C. M., et al. 2008, *ApJ*, 686, 310, doi: [10.1086/591070](https://doi.org/10.1086/591070)
- Hughes, V. A., & Wouterloot, J. G. A. 1984, *ApJ*, 276, 204, doi: [10.1086/161603](https://doi.org/10.1086/161603)
- Hunter, T. R., Brogan, C. L., Indebetouw, R., & Cyganowski, C. J. 2008, *ApJ*, 680, 1271, doi: [10.1086/588016](https://doi.org/10.1086/588016)
- Iglesias, E. 1977, *ApJ*, 218, 697, doi: [10.1086/155727](https://doi.org/10.1086/155727)
- Immer, K., Galván-Madrid, R., König, C., Liu, H. B., & Menten, K. M. 2014, *A&A*, 572, A63, doi: [10.1051/0004-6361/201423780](https://doi.org/10.1051/0004-6361/201423780)
- Immer, K., Reid, M. J., Menten, K. M., Brunthaler, A., & Dame, T. M. 2013, *A&A*, 553, A117, doi: [10.1051/0004-6361/201220793](https://doi.org/10.1051/0004-6361/201220793)
- Jackson, J. M., Rathborne, J. M., Foster, J. B., et al. 2013, *PASA*, 30, e057, doi: [10.1017/pasa.2013.37](https://doi.org/10.1017/pasa.2013.37)
- James, T. A., Viti, S., Holdship, J., & Jiménez-Serra, I. 2020, *A&A*, 634, A17, doi: [10.1051/0004-6361/201936536](https://doi.org/10.1051/0004-6361/201936536)
- Jiménez-Serra, I., Martín-Pintado, J., Báez-Rubio, A., Patel, N., & Thum, C. 2011, *ApJL*, 732, L27, doi: [10.1088/2041-8205/732/2/L27](https://doi.org/10.1088/2041-8205/732/2/L27)
- Jones, L. H., Shoolery, J. N., Shulman, R. G., & Yost, D. M. 1950, *JChPh*, 18, 990, doi: [10.1063/1.1747827](https://doi.org/10.1063/1.1747827)
- Kalenskii, S. V., Promyslov, V. G., & Winnberg, A. 2007, *Astronomy Reports*, 51, 44, doi: [10.1134/S1063772907010052](https://doi.org/10.1134/S1063772907010052)
- Kelly, G., Viti, S., García-Burillo, S., et al. 2017, *A&A*, 597, A11, doi: [10.1051/0004-6361/201628946](https://doi.org/10.1051/0004-6361/201628946)
- Keto, E. R., & Ho, P. T. P. 1989, *ApJ*, 347, 349, doi: [10.1086/168123](https://doi.org/10.1086/168123)

- Khan, S., Pandian, J. D., Lal, D. V., et al. 2022, *A&A*, 664, A140, doi: [10.1051/0004-6361/202140914](https://doi.org/10.1051/0004-6361/202140914)
- Kohno, M., Torii, K., Tachihara, K., et al. 2018, *PASJ*, 70, S50, doi: [10.1093/pasj/psx137](https://doi.org/10.1093/pasj/psx137)
- Kohno, M., Omodaka, T., Handa, T., et al. 2022, *PASJ*, 74, 545, doi: [10.1093/pasj/psac014](https://doi.org/10.1093/pasj/psac014)
- Kurayama, T., Nakagawa, A., Sawada-Satoh, S., et al. 2011, *PASJ*, 63, 513, doi: [10.1093/pasj/63.3.513](https://doi.org/10.1093/pasj/63.3.513)
- Kurtz, S., Hofner, P., & Álvarez, C. V. 2004, *ApJS*, 155, 149, doi: [10.1086/423956](https://doi.org/10.1086/423956)
- Li, J., Wang, J. Z., Gu, Q. S., & Zheng, X. W. 2013, *A&A*, 555, A18, doi: [10.1051/0004-6361/201220943](https://doi.org/10.1051/0004-6361/201220943)
- Li, S., Wang, J., Fang, M., et al. 2019, *ApJ*, 878, 29, doi: [10.3847/1538-4357/ab1e4c](https://doi.org/10.3847/1538-4357/ab1e4c)
- Lis, D. C., Keene, J., Young, K., et al. 1997, *Icarus*, 130, 355, doi: [10.1006/icar.1997.5833](https://doi.org/10.1006/icar.1997.5833)
- Liu, S.-Y., Su, Y.-N., Zinchenko, I., Wang, K.-S., & Wang, Y. 2018, *ApJL*, 863, L12, doi: [10.3847/2041-8213/aad63a](https://doi.org/10.3847/2041-8213/aad63a)
- Mangum, J. G., & Shirley, Y. L. 2015, *PASP*, 127, 266, doi: [10.1086/680323](https://doi.org/10.1086/680323)
- Mendoza, E., Lefloch, B., Ceccarelli, C., et al. 2018, *MNRAS*, 475, 5501, doi: [10.1093/mnras/sty180](https://doi.org/10.1093/mnras/sty180)
- Miettinen, O. 2014, *A&A*, 562, A3, doi: [10.1051/0004-6361/201322596](https://doi.org/10.1051/0004-6361/201322596)
- Minier, V., Peretto, N., Longmore, S. N., et al. 2007, in *Triggered Star Formation in a Turbulent ISM*, ed. B. G. Elmegreen & J. Palous, Vol. 237, 160–164, doi: [10.1017/S1743921307001391](https://doi.org/10.1017/S1743921307001391)
- Miralles, M. P., Rodríguez, L. F., & Scalise, E. 1994, *ApJS*, 92, 173, doi: [10.1086/191965](https://doi.org/10.1086/191965)
- Miralles, M. P., Salas, L., Cruz-González, I., & Kurtz, S. 1997, *ApJ*, 488, 749, doi: [10.1086/304713](https://doi.org/10.1086/304713)
- Moscadelli, L., Reid, M. J., Menten, K. M., et al. 2009, *ApJ*, 693, 406, doi: [10.1088/0004-637X/693/1/406](https://doi.org/10.1088/0004-637X/693/1/406)
- Motte, F., Bontemps, S., & Louvet, F. 2018, *ARA&A*, 56, 41, doi: [10.1146/annurev-astro-091916-055235](https://doi.org/10.1146/annurev-astro-091916-055235)
- Müller, H. S. P., Schlöder, F., Stutzki, J., & Winnewisser, G. 2005, *Journal of Molecular Structure*, 742, 215, doi: [10.1016/j.molstruc.2005.01.027](https://doi.org/10.1016/j.molstruc.2005.01.027)
- Müller, H. S. P., Thorwirth, S., Roth, D. A., & Winnewisser, G. 2001, *A&A*, 370, L49, doi: [10.1051/0004-6361:20010367](https://doi.org/10.1051/0004-6361:20010367)
- Navarete, F., Leurini, S., Giannetti, A., et al. 2019, *A&A*, 622, A135, doi: [10.1051/0004-6361/201629777](https://doi.org/10.1051/0004-6361/201629777)
- Nguyen-Luong, Q., Nakamura, F., Sugitani, K., et al. 2020, *ApJ*, 891, 66, doi: [10.3847/1538-4357/ab700a](https://doi.org/10.3847/1538-4357/ab700a)
- Nguyen-Q-Rieu, Henkel, C., Jackson, J. M., & Mauersberger, R. 1991, *A&A*, 241, L33
- Panagia, N. 1973, *AJ*, 78, 929, doi: [10.1086/111498](https://doi.org/10.1086/111498)
- Peretto, N., & Fuller, G. A. 2009, *A&A*, 505, 405, doi: [10.1051/0004-6361/200912127](https://doi.org/10.1051/0004-6361/200912127)
- Pety, J. 2005, in *SF2A-2005: Semaine de l’Astrophysique Française*, ed. F. Casoli, T. Contini, J. M. Hameury, & L. Pagani, 721
- Povich, M. S., Churchwell, E., Bieging, J. H., et al. 2009, *ApJ*, 696, 1278, doi: [10.1088/0004-637X/696/2/1278](https://doi.org/10.1088/0004-637X/696/2/1278)
- Puga, E., Marín-Franch, A., Najarro, F., et al. 2010, *A&A*, 517, A2, doi: [10.1051/0004-6361/200913294](https://doi.org/10.1051/0004-6361/200913294)
- Purcell, C. R., Balasubramanyam, R., Burton, M. G., et al. 2006, *MNRAS*, 367, 553, doi: [10.1111/j.1365-2966.2005.09921.x](https://doi.org/10.1111/j.1365-2966.2005.09921.x)
- Qiu, K., Zhang, Q., & Menten, K. M. 2011, *ApJ*, 728, 6, doi: [10.1088/0004-637X/728/1/6](https://doi.org/10.1088/0004-637X/728/1/6)
- Quan, D., Herbst, E., Osamura, Y., & Roueff, E. 2010, *ApJ*, 725, 2101, doi: [10.1088/0004-637X/725/2/2101](https://doi.org/10.1088/0004-637X/725/2/2101)
- Quénard, D., Jiménez-Serra, I., Viti, S., Holdship, J., & Coutens, A. 2018, *MNRAS*, 474, 2796, doi: [10.1093/mnras/stx2960](https://doi.org/10.1093/mnras/stx2960)
- Rathborne, J. M., Jackson, J. M., Chambers, E. T., et al. 2005, *ApJL*, 630, L181, doi: [10.1086/491656](https://doi.org/10.1086/491656)
- Rathborne, J. M., Jackson, J. M., & Simon, R. 2006, *ApJ*, 641, 389, doi: [10.1086/500423](https://doi.org/10.1086/500423)
- Reid, M. J., Menten, K. M., Brunthaler, A., et al. 2014, *ApJ*, 783, 130, doi: [10.1088/0004-637X/783/2/130](https://doi.org/10.1088/0004-637X/783/2/130)
- Riffel, R. A., & Lüdke, E. 2010, *MNRAS*, 404, 1449, doi: [10.1111/j.1365-2966.2010.16355.x](https://doi.org/10.1111/j.1365-2966.2010.16355.x)
- Rodríguez, L. F., Garay, G., Curiel, S., et al. 1994, *ApJL*, 430, L65, doi: [10.1086/187439](https://doi.org/10.1086/187439)
- Rodríguez-Fernández, N. J., Tafalla, M., Gueth, F., & Bachiller, R. 2010, *A&A*, 516, A98, doi: [10.1051/0004-6361/201013997](https://doi.org/10.1051/0004-6361/201013997)
- Rygl, K. L. J., Brunthaler, A., Reid, M. J., et al. 2010, *A&A*, 511, A2, doi: [10.1051/0004-6361/200913135](https://doi.org/10.1051/0004-6361/200913135)
- Sánchez-Monge, Á., López-Sepulcre, A., Cesaroni, R., et al. 2013, *A&A*, 557, A94, doi: [10.1051/0004-6361/201321589](https://doi.org/10.1051/0004-6361/201321589)
- Sandell, G., Wright, M., Güsten, R., et al. 2020, *ApJ*, 904, 139, doi: [10.3847/1538-4357/abbf5b](https://doi.org/10.3847/1538-4357/abbf5b)
- Sanhueza, P., Garay, G., Bronfman, L., et al. 2010, *ApJ*, 715, 18, doi: [10.1088/0004-637X/715/1/18](https://doi.org/10.1088/0004-637X/715/1/18)
- Sanhueza, P., Jackson, J. M., Foster, J. B., et al. 2012, *ApJ*, 756, 60, doi: [10.1088/0004-637X/756/1/60](https://doi.org/10.1088/0004-637X/756/1/60)
- Sato, M., Wu, Y. W., Immer, K., et al. 2014, *ApJ*, 793, 72, doi: [10.1088/0004-637X/793/2/72](https://doi.org/10.1088/0004-637X/793/2/72)
- Sharpless, S. 1959, *ApJS*, 4, 257, doi: [10.1086/190049](https://doi.org/10.1086/190049)
- Shepherd, D. S., Nürnberger, D. E. A., & Bronfman, L. 2004, *ApJ*, 602, 850, doi: [10.1086/381050](https://doi.org/10.1086/381050)
- Shepherd, D. S., Povich, M. S., Whitney, B. A., et al. 2007, *ApJ*, 669, 464, doi: [10.1086/521331](https://doi.org/10.1086/521331)
- Shirley, Y. L. 2015, *PASP*, 127, 299, doi: [10.1086/680342](https://doi.org/10.1086/680342)

- Simon, R., Rathborne, J. M., Shah, R. Y., Jackson, J. M., & Chambers, E. T. 2006, *ApJ*, 653, 1325, doi: [10.1086/508915](https://doi.org/10.1086/508915)
- Snell, R. L., & Bally, J. 1986, *ApJ*, 303, 683, doi: [10.1086/164117](https://doi.org/10.1086/164117)
- Snyder, L. E., & Buhl, D. 1971, *ApJL*, 163, L47, doi: [10.1086/180664](https://doi.org/10.1086/180664)
- Sollins, P. K., Hunter, T. R., Battat, J., et al. 2004, *ApJL*, 616, L35, doi: [10.1086/421294](https://doi.org/10.1086/421294)
- Su, Y.-N., Liu, S.-Y., Chen, H.-R., & Tang, Y.-W. 2012, *ApJL*, 744, L26, doi: [10.1088/2041-8205/744/2/L26](https://doi.org/10.1088/2041-8205/744/2/L26)
- Tideswell, D. M., Fuller, G. A., Millar, T. J., & Markwick, A. J. 2010, *A&A*, 510, A85, doi: [10.1051/0004-6361/200810820](https://doi.org/10.1051/0004-6361/200810820)
- Urquhart, J. S., Figura, C., Wyrowski, F., et al. 2019, *MNRAS*, 484, 4444, doi: [10.1093/mnras/stz154](https://doi.org/10.1093/mnras/stz154)
- Vasyunina, T., Linz, H., Henning, T., et al. 2011, *A&A*, 527, A88, doi: [10.1051/0004-6361/201014974](https://doi.org/10.1051/0004-6361/201014974)
- Velilla Prieto, L., Sánchez Contreras, C., Cernicharo, J., et al. 2015, *A&A*, 575, A84, doi: [10.1051/0004-6361/201424768](https://doi.org/10.1051/0004-6361/201424768)
- Vlemmings, W. H. T., Diamond, P. J., van Langevelde, H. J., & Torrelles, J. M. 2006, *A&A*, 448, 597, doi: [10.1051/0004-6361:20054275](https://doi.org/10.1051/0004-6361:20054275)
- Vlemmings, W. H. T., Surcis, G., Torstensson, K. J. E., & van Langevelde, H. J. 2010, *MNRAS*, 404, 134, doi: [10.1111/j.1365-2966.2010.16297.x](https://doi.org/10.1111/j.1365-2966.2010.16297.x)
- Wang, Y., Beuther, H., Bik, A., et al. 2011, *A&A*, 527, A32, doi: [10.1051/0004-6361/201015543](https://doi.org/10.1051/0004-6361/201015543)
- Watson, C., Churchwell, E., Zweibel, E. G., & Crutcher, R. M. 2007, *ApJ*, 657, 318, doi: [10.1086/510547](https://doi.org/10.1086/510547)
- Westerhout, G. 1958, *BAN*, 14, 215
- Wienen, M., Wyrowski, F., Schuller, F., et al. 2012, *A&A*, 544, A146, doi: [10.1051/0004-6361/201118107](https://doi.org/10.1051/0004-6361/201118107)
- Wilson, T. L., & Rood, R. 1994, *ARA&A*, 32, 191, doi: [10.1146/annurev.aa.32.090194.001203](https://doi.org/10.1146/annurev.aa.32.090194.001203)
- Wynn-Williams, C. G., Becklin, E. E., & Neugebauer, G. 1974, *ApJ*, 187, 473, doi: [10.1086/152656](https://doi.org/10.1086/152656)
- Xie, J., Fuller, G. A., Li, D., et al. 2021, *Science China Physics, Mechanics, and Astronomy*, 64, 279511, doi: [10.1007/s11433-021-1695-0](https://doi.org/10.1007/s11433-021-1695-0)
- Xu, Y., Moscadelli, L., Reid, M. J., et al. 2011, *ApJ*, 733, 25, doi: [10.1088/0004-637X/733/1/25](https://doi.org/10.1088/0004-637X/733/1/25)
- Xu, Y., Li, J. J., Reid, M. J., et al. 2013, *ApJ*, 769, 15, doi: [10.1088/0004-637X/769/1/15](https://doi.org/10.1088/0004-637X/769/1/15)
- Yan, Y. T., Henkel, C., Kobayashi, C., et al. 2022, *arXiv e-prints*, arXiv:2212.03252, <https://arxiv.org/abs/2212.03252>
- Zapata, L. A., Fernandez-Lopez, M., Curiel, S., Patel, N., & Rodriguez, L. F. 2013, *arXiv e-prints*, arXiv:1305.4084, doi: [10.48550/arXiv.1305.4084](https://doi.org/10.48550/arXiv.1305.4084)
- Zemlyanukha, P. M., Zinchenko, I. I., Salii, S. V., Ryabukhina, O. L., & Liu, S. Y. 2018, *Astronomy Reports*, 62, 326, doi: [10.1134/S1063772918050074](https://doi.org/10.1134/S1063772918050074)
- Zhang, X., Quan, D., Chang, Q., et al. 2020, *MNRAS*, 497, 609, doi: [10.1093/mnras/staa1979](https://doi.org/10.1093/mnras/staa1979)
- Zinchenko, I., Henkel, C., & Mao, R. Q. 2000, *A&A*, 361, 1079, <https://arxiv.org/abs/astro-ph/0007095>
- Zinchenko, I., Liu, S. Y., Su, Y. N., et al. 2012, *ApJ*, 755, 177, doi: [10.1088/0004-637X/755/2/177](https://doi.org/10.1088/0004-637X/755/2/177)
- . 2015, *ApJ*, 810, 10, doi: [10.1088/0004-637X/810/1/10](https://doi.org/10.1088/0004-637X/810/1/10)